Power Electronic Systems
Laboratory

© 2016 IEEE

Proceedings of the 42nd Annual Conference of the IEEE Industrial Electronics Society (IECON 2016), Florence, Italy, October 23-27, 2016

Outrunner Generator with Optimized Cogging Torque Pattern for an Electromechanical Energy Harvester

M. Flankl,
A. Tüysüz,
J. W. Kolar

This material is published in order to provide access to research results of the Power Electronic Systems Laboratory / D-ITET / ETH Zurich. Internal or personal use of this material is permitted. However, permission to reprint/republish this material for advertising or promotional purposes or for creating new collective works for resale or redistribution must be obtained from the copyright holder. By choosing to view this document, you agree to all provisions of the copyright laws protecting it.

Eidgenössische Technische Hochschule Zürich
Swiss Federal Institute of Technology Zurich

Outrunner Generator with Optimized Cogging Torque Pattern for an Electromechanical Energy Harvester

Michael Flankl, Arda Tüysüz and Johann W. Kolar
Power Electronic Systems Laboratory
Swiss Federal Institute of Technology (ETH Zurich),
Physikstrasse 3
8092 Zurich, Switzerland

Abstract— **In contrast to widely applied permanent magnet (PM) machine optimization for minimization of cogging torque, this paper describes a method for shaping the cogging torque of a PM outrunner machine towards a desired sinusoidal torque pattern. The underlying goal of this approach is to compensate the cogging torque of a kinetic energy harvester (KEH) with the optimized counter cogging torque of a generator connected to the same shaft. Therefore, the total cogging torque is highly reduced, and a self-starting electromechanical energy harvester, comprising KEH and outrunner generator is formed. The key degree of freedom for shaping the cogging torque is the sinusoidal modulation of the machine's air gap. An algorithm based on the multi-dimensional Secant method, which is related to the multi-dimensional Newton-Raphson method, first evaluates the cogging torque of a given generator geometry with two-dimensional finite element method (2-D FEM) simulations and then iterates the geometry of the outrunner machine until the cogging torque target is achieved. Using the presented optimization approach, a generator design with the desired sinusoidal cogging torque pattern is obtained, achieving a total cogging torque reduction of the overall electromechanical energy harvesting system of 90%.**

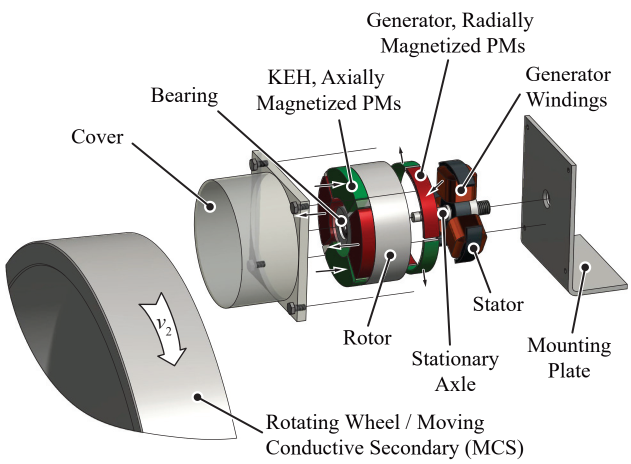

Fig. 1: Electromechanical energy harvester with the integrated outrunner generator. The generator exhibits an optimized cogging torque pattern, which compensates the cogging torque of the kinetic energy harvester (KEH). It leads to a self-starting capability of the overall harvester setup.

I. Introduction

The cogging torque (detent torque) in conventional permanent magnet (PM) machines occurs due to a reluctance variation along the stator perimeter introduced by the stator teeth in combination with the PMs. It is even present without stator excitation [1] and typically, a minimization of the cogging torque is targeted in the course of machine design. This topic is widely analyzed for DC machines [2], permanent magnet synchronous machines (PMSM) [3–11] and brushless DC (BLDC) machines [12–14] in recent publications and in textbooks [1, 15, 16]. However, for certain applications as described in [17] and for the kinetic energy harvester (KEH) discussed in this paper, a specially shaped, non-vanishing cogging torque is desired.

The electromechanical energy harvester introduced in [18] harvests electrical energy/power without mechanical contact, from the kinetic energy/power of a moving conductive secondary (MCS). The system overview is given in Fig. 2. It comprises a KEH and a generator, that converts the harvested

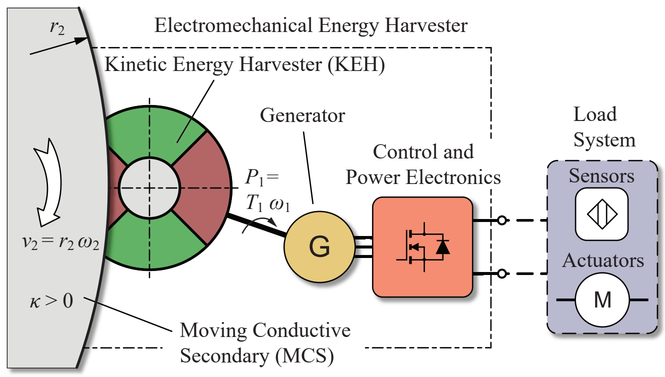

Fig. 2: System overview of the electromechanical energy harvester introduced in [18].

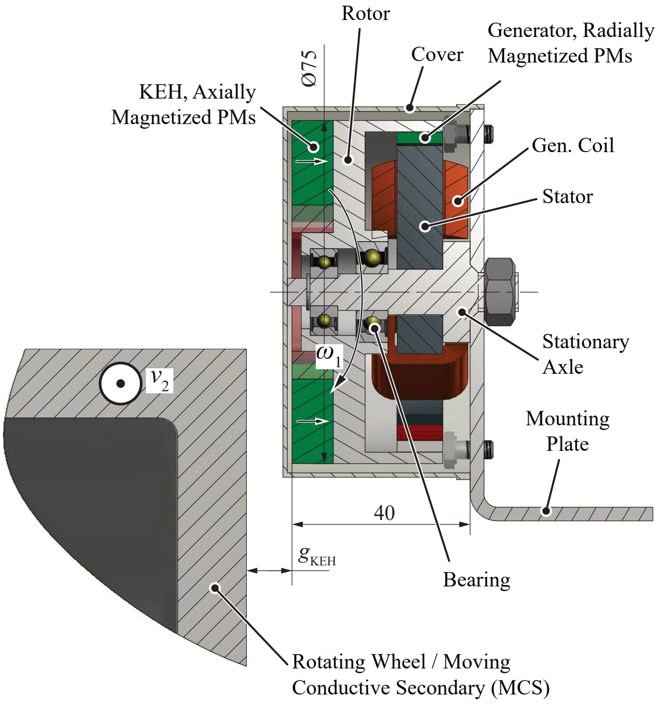

Fig. 3: Cross section of the electromechanical energy harvester, showing actual geometric dimensions and the compact composition of the electromechanical energy harvester with integrated outrunner generator.

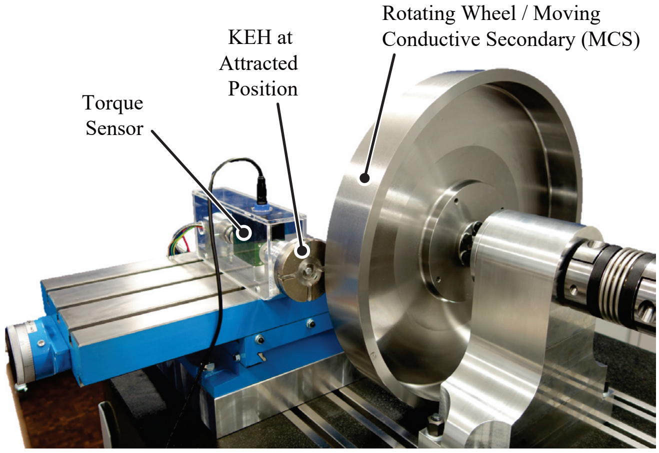

Fig. 4: Setup for measuring the KEH cogging torque. The partial overlap of KEH and MCS gives a magnetically favorable position at its energetic minimum, which is shown in the picture.

kinetic energy/power to electric energy/power. The prototype presented in [18] harvests from an aluminum MCS and utilizes an off-the-shelf generator. In order to broaden the range of possible applications, it is desired to also allow MCSs made of a ferromagnetic material, e.g. steel.

A. System start-up

Measurements show that the KEH based on [18] can harvest a mechanical power of $P_{\text{mech}} \approx 10\,\text{W}$ in the steady-state operation at an air gap $g_{\text{KEH}} = 10\,\text{mm}$, when the speed of the MCS made of C45E steel is $v_2 = 22\,\text{m/s}$. However, the use of a MCS made of steel leads to an effect, which is not present when an aluminum MCS [18] is used. Due to the inherent partial overlap of KEH and MCS (cf. Fig. 2), a magnetically favorable rotational position of the KEH appears at standstill. In other words, a KEH, optimized for high energy harvesting capability, exhibits a high cogging torque. The cogging torque of the KEH of [18], depicted in Fig. 5, is calculated as a function of angular position with the aid of 3-D finite element method (FEM) simulations and verified with a precision torque sensor mounted on the same shaft as the KEH (cf. Fig. 4).

Literature [19–22] proposes electrical compensation of torque ripple and cogging torque of electrical machines. For the energy harvesting system as depicted in Fig. 2, this would mean to drive the generator in motor mode for the system start-up in order to overcome the KEH cogging torque. Consequently, energy from an external energy storage would be required to start up the energy harvester. Moreover, a control would be required to identify whether energy harvesting is possible (i.e. to detect if the MCS is in motion) or not (MCS not in motion; system shut down). However, for applying the proposed electromechanical energy harvesting system in industry, a self-start-up capability is highly beneficial, leading to the key idea of this work. If the generator (cf. Fig. 2) has the same amount, but opposite sign of cogging torque as the KEH for each rotational point, the total cogging torque of KEH *and* generator vanishes,

$$\begin{aligned} T_{\text{cog,gen}}(\varphi) + T_{\text{cog,harv}}(\varphi) &\overset{!}{=} 0 \\ \Rightarrow T_{\text{cog,gen}}(\varphi) &= -T_{\text{cog,harv}}(\varphi)\,. \end{aligned} \tag{1}$$

B. Electromechanical energy harvester with integrated outrunner generator

Since the KEH has a disk-shaped geometry, the generator is beneficially implemented as an outrunner machine. This leads to a highly compact design as depicted in Fig. 1 and Fig. 3. The axially magnetized KEH PMs and the radially magnetized generator PMs are mounted on a pot-shaped steel rotor. It is intended to use different PMs for KEH and generator as it conveniently allows to decouple both machine designs. The rotor forms a yoke for all placed PMs and is of solid steel as it experiences negligible flux variation during operation. The stator, on the other hand, is made of laminated electrical steel.

This paper proposes the cogging torque cancelation of an already introduced kinetic energy harvester [18] with the counter cogging torque of an optimized PM outrunner machine. Sec. II

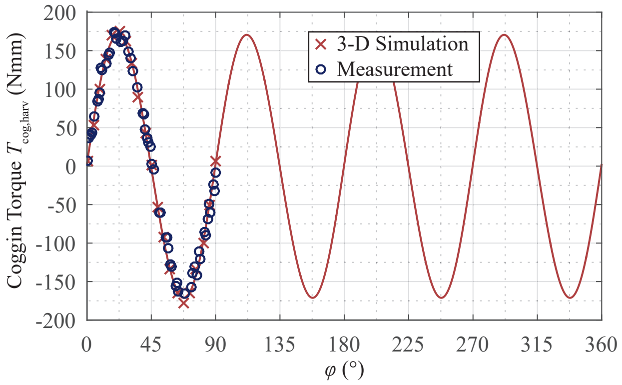

Fig. 5: Cogging torque of the KEH obtained by measurements and 3-D FEM simulation. The cogging torque is sinusoidal and has a mechanical period of 90°.

derives the concept of cogging torque shaping on an example with a slotless stator. In a next step, an iterative method for shaping the cogging torque of the outrunner machine towards a desired pattern is introduced in Sec. III. Simulation results and a machine design yielded by the optimization procedure are presented in Sec. IV, and the electrical performance of the optimized generator is analyzed in Sec. V. Finally, Sec. VI summarizes the main results and identifies topics of future research.

II. Cogging Torque of Slotless Stator

As depicted in Fig. 5, the cogging torque of the KEH and therefore the desired inverse cogging torque of the generator can be approximated well with a sinusoidal function, exhibiting a period of 90° mechanical rotation. Prior to the actual stator optimization procedure in Sec. III, the approach is derived with the cogging torque analysis of a slotless (and windingless) stator.

Specially shaped magnets as proposed in [5] and magnets with variable width as proposed in [4] are excluded from the consideration as this would lead to mechanical unbalance, increased mounting effort and increased PM costs. Hence, only radially magnetized sector magnets are considered for the generator. A specific stator shape, resulting from the modulation of the air gap, is selected as the most suitable degree of freedom for the cogging torque shaping. Since the stator is made of laminated electrical steel and the individual sheets are laser cut in a prototyping process and punched in mass production, the optimized stator shape has negligible additional production cost compared to a conventional outrunner machine of similar size.

The cogging torque, either obtained by FEM simulations or analytical derivations, can be expressed with a Fourier

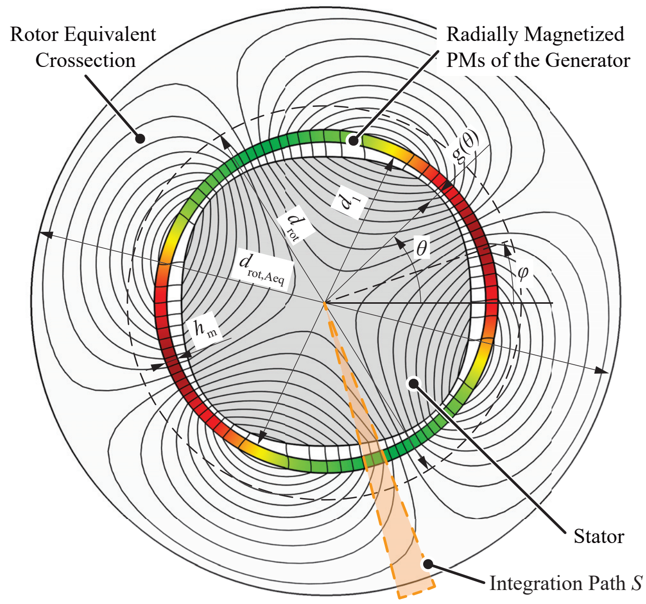

Fig. 6: 2-D FEM simulation of a slotless generator configuration, achieving the desired sinusoidal cogging torque pattern. The key design tool for shaping the cogging torque is the sinusoidal modulation of the air gap $g(\theta)$ and magnetization $B_{\mathrm{rem,r}}(\theta)$. In order to represent the pot-shaped geometry of the rotor in this 2-D simulation, the rotor is modeled with an area equivalent diameter $d_{\mathrm{rot,Aeq}}$.

expansion

$$\begin{aligned} T_{\mathrm{cog}}(\varphi) = & c_1 \sin(4\,\varphi) + d_1 \cos(4\,\varphi) \\ & + c_2 \sin(8\,\varphi) + d_2 \cos(8\,\varphi) \ldots , \end{aligned} \tag{2}$$

where φ is the angle of rotational position. As it is desired (cf. (1)) to obtain a torque, shaped as the KEH torque in Fig. 5, but opposite in sign, all components in (2) except for c_1 should vanish.

A slotless stator geometry in combination with a sinusoidal PM magnetization that leads to the desired sinusoidal cogging torque is depicted in Fig. 6. The air gap modulation $g(\theta)$ and the PM's remanent flux density $B_{\mathrm{rem,r}}(\theta, \varphi)$ are of the form

$$g(\theta) = g_{\mathrm{nom}} \cdot (1 + a_1 \cos(4\,\theta)) \tag{3a}$$

$$B_{\mathrm{rem,r}}(\theta, \varphi) = B_{\mathrm{rem}} \cos(2\,(\theta - \varphi)) , \tag{3b}$$

where θ is the geometric angle in the stator coordinate system and $B_{\mathrm{rem}} = 1.4\,\mathrm{T}$ for this analysis.

In a similar consideration as in [23], by applying Ampere's law

$$\oint_S \frac{\vec{B}}{\mu} \mathrm{d}\vec{s} = \int_A \vec{j}\, \mathrm{d}\vec{A} , \tag{4}$$

on any integration path (one is indicated in Fig. 6) including stator, air gap, PMs and the rotor and with assuming $\mu_{\mathrm{Fe}} \to \infty$, $\mu_{\mathrm{PM}} = \mu_0$, the flux density in the air gap in radial direction

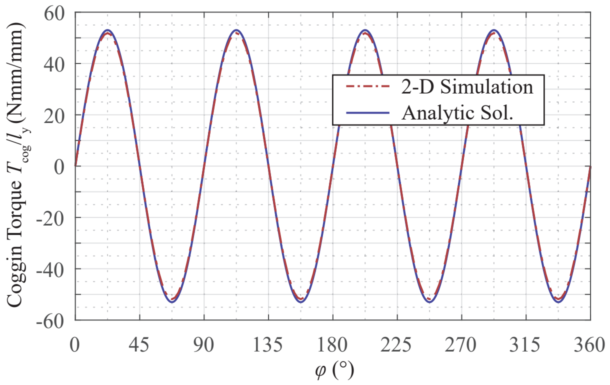

Fig. 7: Sinusoidal cogging torque of a slotless generator configuration; per length in axial direction l_{y}. Almost no deviation between the torque predicted by the derived analytic model and the 2-D FEM simulation results can be observed. Parameters of shown results are $B_{\mathrm{rem}} = 1.4\,\mathrm{T}$, $g_{\mathrm{nom}} = 2\,\mathrm{mm}$, $a_1 = 0.5$, $h_{\mathrm{m}} = 2.5\,\mathrm{mm}$, $d_1 = 65\,\mathrm{mm}$.

can be calculated as

$$B_{\mathrm{r}}(\theta,\varphi) = \frac{B_{\mathrm{rem,r}}(\theta,\varphi)}{{}^{g(\theta)}/_{h_m} + 1} \,. \tag{5}$$

The total magnetic energy, stored in in air gap and PMs only, can then be calculated as

$$W_{\mathrm{m}}(\varphi) = l_{\mathrm{y}} \int_0^{2\pi} \frac{B_{\mathrm{r}}^2(\theta,\varphi)}{2\,\mu_0} \cdot (h_m + g(\theta)) \cdot \underbrace{({}^{d_1}/_2 - {}^{g(\theta)}/_2)}_{r(\theta)} \,\mathrm{d}\theta \,, \tag{6}$$

where l_{y} is the axial length and h_{m} the radial magnet height.

Finally, the cogging torque acting on the rotor can be obtained as the derivative of the magnetic energy in air gap and PMs $W_{\mathrm{m}}(\varphi)$ with respect to the angle of rotational position φ

$$T_{\mathrm{cog}}(\varphi) = -\frac{\partial W_{\mathrm{m}}(\varphi)}{\partial \varphi} = c_1\, \sin(4\,\varphi) \,, \tag{7}$$

where c_1 can be expressed as

$$\begin{aligned} c_1 =& l_{\mathrm{y}}\, \pi\, B_{\mathrm{r}}^2\, h_{\mathrm{m}}^2\, (d_1 + h_{\mathrm{m}}) \cdot \\ & \frac{g_{\mathrm{nom}}\,(\gamma + a_1 - 1) - h_{\mathrm{m}}\,(1-\gamma)}{\mu_0\, a_1\, g_{\mathrm{nom}}(g_{\mathrm{nom}}\,(1-a_1) + h_{\mathrm{m}})} \,, \end{aligned} \tag{8}$$

with

$$\gamma = \sqrt{1 - \frac{2\,a_1}{1 + a_1 + {}^{h_{\mathrm{m}}}/_{g_{\mathrm{nom}}}}} \,.$$

Finally, Fig. 7 verifies the analytic cogging torque calculation of a slotless arrangement (cf. Fig. 6) with 2-D FEM simulations.

Obviously, the concept of air gap modulation can be extended by adding introducing terms, such that

$$g(\theta) = g_{\mathrm{nom}} \cdot (1 + \sum_{i=1}^{n} a_i\, \cos(4\,i\,\theta) + b_i\, \sin(4\,i\,\theta)) \tag{9}$$

is the basis for optimizing the air gap geometry. In that case, the resulting cogging torque is represented in the following as

$$T_{\mathrm{cog}}(\varphi) = \sum_{i=1}^{n} c_i\, \sin(4\,i\,\varphi) + d_i\, \cos(4\,i\,\varphi) \,. \tag{10}$$

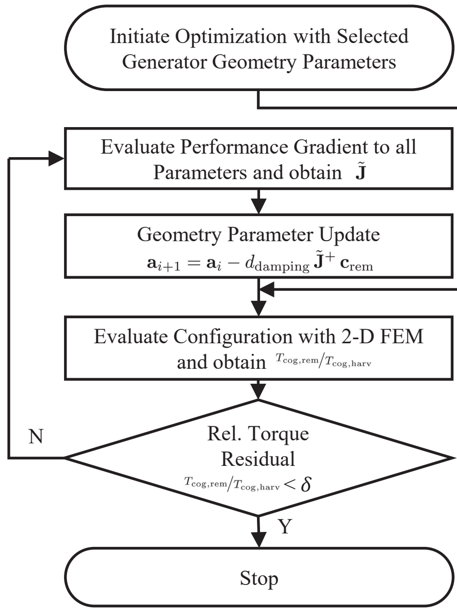

Fig. 8: Flowchart depicting the iterative optimization algorithm. The optimization is based on a multi-dimensional Secant Method, which is related to the multi-dimensional Newton-Raphson Method, first evaluates the cogging torque of the current generator geometry with 2-D FEM simulations and then iterates the geometry of the outrunner machine until the cogging torque target is achieved. The iteration loop is left when the relative residual is sufficiently small ${}^{T_{\mathrm{cog,rem}}}/_{T_{\mathrm{cog,harv}}} < \delta = 0.1$.

III. Cogging Torque Pattern Optimization

The optimization is initialized based on the findings obtained from the slotless arrangement, depicted in Fig. 9 (a) and with simulation parameters according to Table I. Clearly, slots (with the angular width of the stator teeth α_{FE}) are introduced for placing the stator coils. Additionally, the sinusoidal PM remanent flux density in Sec. II is replaced by PMs with constant PM remanent flux density $B_{\mathrm{rem,r}}(\theta,\varphi) = B_{\mathrm{rem}} = 1.4\,\mathrm{T}$, where an angular gap between the PMs α_{PMgap} is introduced and part of the optimization.

A. Optimization Algorithm

A flowchart depicting the optimization algorithm is given in Fig. 8. After initializing the optimization with selected

TABLE I: Parameters used for the 2-D FEM simulations of the generator.

Parameter	Variable	Value
Generator bore diameter	d_1	67 mm
PM height	h_{PM}	1.5 mm
2-D rotor diameter[a]	$d_{\mathrm{rot,Aeq}}$	120 mm
Actual rotor diameter	d_{rot}	75 mm
Stator material		M235-35A
Rotor rel. permeability	$\mu_{\mathrm{rot,rel}}$	700
Stator width	l_{y}	10 mm
Number of pole pairs	p	2
Number of phases	m	3
Nominal air gap	g_{nom}	2 mm
PM remanent flux density	B_{rem}	1.4 T
PM rel. permeability	$\mu_{\mathrm{PM,rel}}$	1.05
Stator tooth width	w_{FE}	10 mm
Coil cross section	A_{coil}	143 mm^3

[a] Used to represent the actually pot-shaped rotor flux path in 2-D simulation.

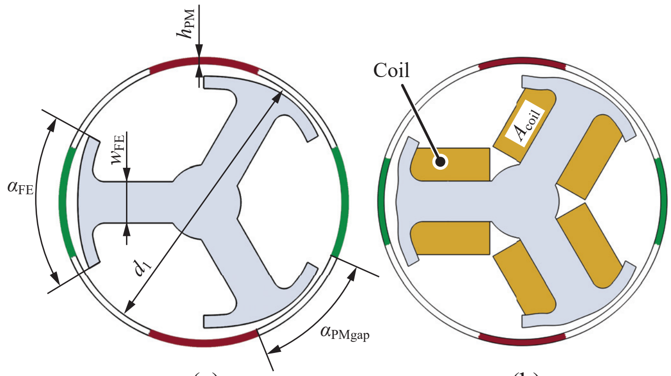

Fig. 9: Outrunner generator geometry. (a) initial geometry fed into the optimization and (b) resulting optimized stator geometry with sinusoidal cogging torque.

geometry parameters, the current configuration is evaluated by calculating the cogging torque as function of the angle of rotational position φ with 2-D FEM simulations. Then, the utilized algorithm iterates the geometry until the cogging torque target is reached. Due to the numerical nature of the simulation, the previously introduced condition for completely vanishing total cogging torque (1) cannot be reached. Therefore, a torque residual

$$T_{\mathrm{cog,rem}} = T_{\mathrm{cog,harv}} - T_{\mathrm{cog,gen}} \tag{11}$$

is computed and the iteration loop is terminated when the relative residual is sufficiently small $T_{\mathrm{cog,rem}}/T_{\mathrm{cog,harv}} < \delta$. In the following optimization procedure, $\delta = 0.1$ is selected as it leads to a sufficient reduction of total cogging torque of 90%.

$T_{\mathrm{cog,harv}}$ and $T_{\mathrm{cog,gen}}$ are functions of the continuous variable φ and therefore intrinsically difficult to handle in an optimization. A decomposition of the cogging torque according to (10) is performed and a vector of cogging torque harmonic components

$$\mathbf{c} = \begin{bmatrix} c_1 & d_1 & \dots & c_m & d_m \end{bmatrix}^{\mathrm{T}} \tag{12}$$

is obtained. A similar decomposition can be performed for $T_{\mathrm{cog,harv}}$ and (11) can be rewritten as

$$\mathbf{c}_{\mathrm{rem}} = \mathbf{c}_{\mathrm{harv}} - \mathbf{c}_{\mathrm{gen}} \ . \tag{13}$$

On the other hand, it is also convenient to represent the geometry parameters in a vector

$$\mathbf{a} = \begin{bmatrix} \alpha_{\mathrm{FE}} & \alpha_{\mathrm{PMgap}} & b_1 & \dots & a_n & b_n \end{bmatrix}^{\mathrm{T}} . \tag{14}$$

The modulation index a_1 (cf. (3)) is not updated during the optimization and is used as an external geometry parameter. It is set $a_1 = 0.5$ in the presented results.

The update of geometry parameters is a multi-dimensional Secant Method, which is related to the multi-dimensional Newton-Raphson Method [24], but utilizes the secant as an approximation for the Jacobian matrix,

$$\frac{\partial \mathbf{c}_i}{\partial \mathbf{a}_j} \approx \tilde{\mathbf{J}} = \begin{bmatrix} \frac{\Delta c_1}{\Delta \alpha_{\mathrm{FE}}} & \cdots & \frac{\Delta c_1}{\Delta b_n} \\ \vdots & \ddots & \vdots \\ \frac{\Delta d_m}{\Delta \alpha_{\mathrm{FE}}} & \cdots & \frac{\Delta d_m}{\Delta b_n} \end{bmatrix} , \tag{15}$$

for finding the root (zero) of the error function ($\mathbf{c}_{\mathrm{rem}}$ here) [25]. For obtaining e.g. the first column in $\tilde{\mathbf{J}}$, the parameter α_{FE} is perturbed and a simulation is conducted. The difference in terms of cogging torque decomposition $\mathbf{c}_{\mathrm{gen}}$ gives the values for the first column. This procedure is conducted for all elements in geometry parameter $\mathbf{a}$, such that $\tilde{\mathbf{J}}$ can be filled.

Then the geometry parameter $\mathbf{a}$ is updated such that the torque residual $\mathbf{c}_{\mathrm{rem}}$ is reduced,

$$\mathbf{a}_{i+1} = \mathbf{a}_i - d_{\mathrm{damping}} \, \tilde{\mathbf{J}}^{+} \, \mathbf{c}_{\mathrm{rem}} \ . \tag{16}$$

The pseudoinverse of the approximated Jacobian matrix,

$$\tilde{\mathbf{J}}^{+} := \left(\tilde{\mathbf{J}}^{\mathrm{T}}\tilde{\mathbf{J}}\right)^{-1} \tilde{\mathbf{J}}^{\mathrm{T}} ,$$

is used for the update step since the existence of $\tilde{\mathbf{J}}^{-1}$ cannot be guaranteed. Due to the strong nonlinearity of the optimization problem, a damping factor d_{damping} is applied in the update step; $d_{\mathrm{damping}} = 0.2$ showed good convergence.

IV. Optimization Results

The cogging torque optimization is conducted for the presented three-phase outrunner generator. Simulation results obtained by a 2-D FEM simulation of the described iterative optimization algorithm are given in the following. In Fig. 9 (a), the initial geometry is shown and Fig. 9 (b) shows the

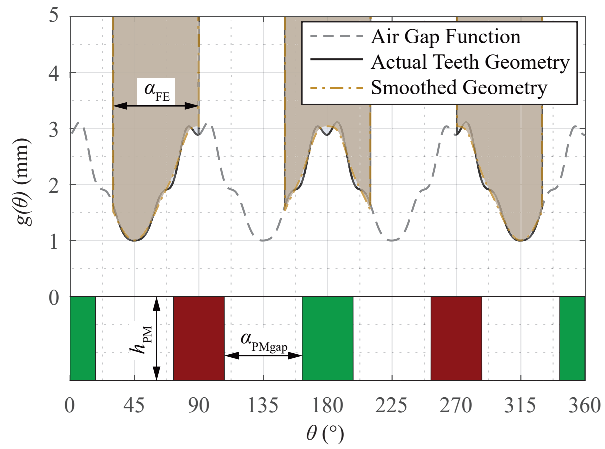

Fig. 10: Illustration of the air gap function and the actual teeth geometry as well as the permanent magnet arrangement for the optimized generator. A post-smoothed geometry is also shown.

TABLE II: Parameters of test setup for experimental results.

Variable	Initial Value	Optimized Value
α_{FE}	60°	59.7°
α_{PMgap}	45°	54.4°
a_1	0.5	0.5
b_1	0	0.0056
a_2	0	0.0245
b_2	0	0.0021
a_3	0	0.0388
b_3	0	0.0073
a_4	0	-0.0356
b_4	0	0.0057
a_5	0	-0.0657
b_5	0	0.0020
a_6	0	-0.0161
b_6	0	0.0030
$a_{i>6}$, $b_{i>6}$	0	0

resulting geometry obtained by the optimization. Moreover, Fig. 10 shows the resulting air gap function and actual teeth geometry of the optimized design in a linear diagram. It can be observed that the gap between the PMs (α_{PMgap}) perceptibly increased, while the stator shape is changed only slightly. A comparison of initial geometry parameters and optimized geometry parameters is given in Table II.

The evolution of cogging torque during the optimization process is depicted in Fig. 11 (for a selected number of designs during the iteration). The optimization converges towards the desired sinusoidal cogging torque, however, the introduced algorithm allows in principle to optimize for any desired cogging torque shape.

A comparison of cogging torques of harvester $T_{\mathrm{cog,harv}}$ and the final design of the generator $T_{\mathrm{cog,gen}}$ is given in Fig. 12. In summary, the conducted 2-D FEM simulations indicate that the presented algorithm allows to reduce the total cogging torque of the total energy harvester, comprising KEH and outrunner generator, by $\approx 90\%$.

A. Post-Smoothed Geometry

In order to explain the influence of higher order air gap modulation components ($a_{i>2}$, $b_{i>2}$) further, the optimized geometry of Fig. 9 (b) is smoothed and its cogging torque is analyzed. Moreover, a rather smooth stator geometry could also be a manufacturing requirement, when the sheets of the stator iron are punched in a mass production.

The smoothing is applied to the optimized air gap function $g(\theta)$, depicted in Fig. 10. The resulting cogging torque curve is shown in Fig. 11 , where a slight deviation to the desired

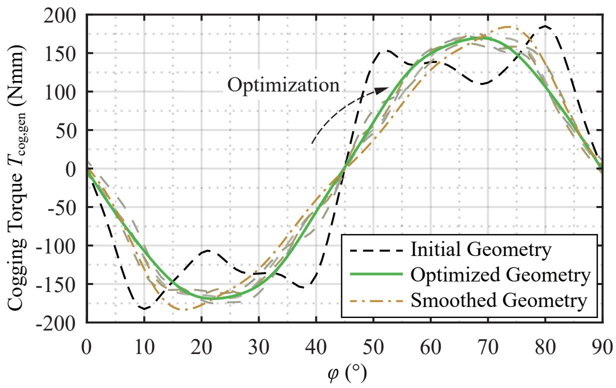

Fig. 11: Generator cogging torque as result of 2-D FEM simulation, indicating the iterative optimization of the introduced algorithm. The optimization converges towards the desired sinusoidal cogging torque, however, the introduced algorithm allows to optimize for any desired cogging torque shape.

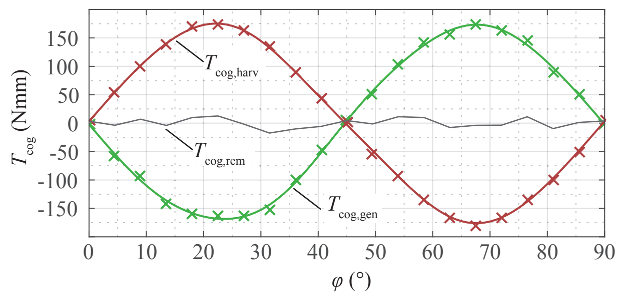

Fig. 12: Compensation of KEH cogging torque ($T_{\mathrm{cog,harv}}$) with optimized counter cogging torque of the outrunner generator ($T_{\mathrm{cog,gen}}$). The 2-D FEM simulation of generator cogging torque shows that a desired sinusoidal cogging torque pattern is achieved with the optimization. $T_{\mathrm{cog,rem}}$ is the resulting total cogging torque of the electromechanical energy harvester, where a reduction of 90%, compared to the cogging torque caused by the KEH ($T_{\mathrm{cog,harv}}$) is achieved.

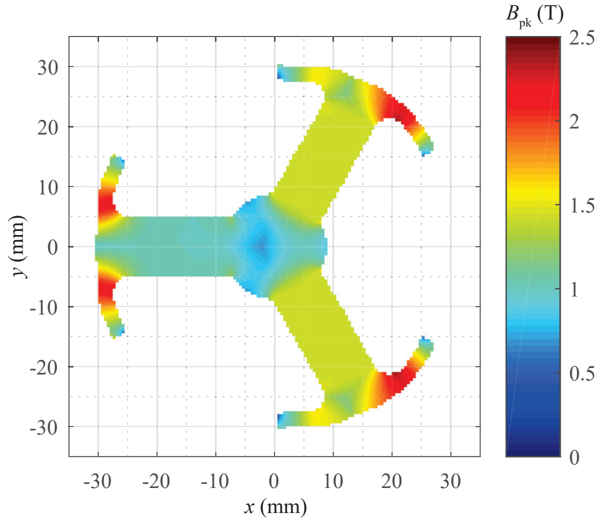

Fig. 13: Map of peak flux density in the stator obtained by 2-D FEM simulation and utilized to compute the iron losses for the efficiency calculation.

sinusoidal form can be noticed. In this case study, smoothing applied on the optimized geometry degraded the cogging torque compensation to $\approx 70\%$.

V. Electrical Performance

The electrical performance of the generator whose cogging torque is optimized in Sec. IV concludes the analysis conducted in this work and will be discussed briefly in the following section.

The generator operation point (OP) is defined by the energy harvesting capability of the KEH. Since various parameters as MCS speed v_2, KEH air gap g_{KEH} (cf. Fig. 3 for both) and MCS material grade are taking influence on the generator's OP, parameters for a nominal OP, based on earlier KEH measurements, are listed in Table III and will serve as a reference OP for characterizing the generator's performance.

The electrical performance of the generator is calculated regarding only two loss components: iron losses and copper losses. Iron losses P_{Fe} are calculated based on the Steinmetz equation, obtained from the loss data provided by a stator manufacturer for the material M235-35A (cf. EN 10106; with $0.35\,\mathrm{mm}$ lamination thickness), as

$$P_{\mathrm{Fe}} = \frac{l_{\mathrm{y}}}{1\,\mathrm{m}} \cdot \int_{A_{\mathrm{stator}}} 45.7\,\mathrm{W/m^3} \cdot \left(\frac{f_{\mathrm{el}}}{1\,\mathrm{Hz}}\right)^{1.30} \cdot \left(\frac{B_{\mathrm{pk}}(A)}{1\,\mathrm{T}}\right)^{1.87} \mathrm{d}A\,, \tag{17}$$

where the peak flux density B_{pk} of every point in the stator (shown in Fig. 13) during one electrical period is extracted from 2-D FEM simulations.

The copper losses P_{cu} are calculated as Joule losses due to the required current, where the direct-component of the current is assumed to be zero ($i_{\mathrm{d}} = 0$) for maximum-torque-per-ampere operation. Since the machine's length is considerably short, end winding losses also contribute significantly ($\approx 50\,\%$) to the copper losses. Proximity losses in the stator windings can be neglected as the distinct T-shape of the stator teeth effectively shields the winding area.

Finally, the generator's efficiency for the nominal OP is calculated as $\eta = 90.5\,\%$, showing that the cogging torque shaping as proposed in this paper does not significantly degrade the performance.

TABLE III: Electrical performance calculation.

Parameter	**Variable**	**Value**
Nominal torque	T_{n}	$45\,\mathrm{Nmm}$
Nominal speed	n_{n}	$2150\,\mathrm{rpm}$
Nominal mechanical power	P_{mech}	$10.1\,\mathrm{W}$
Winding cross-section	A_{winding}	$143\,\mathrm{mm}^2$
Filling factor	k_{cu}	0.65
Total copper volume	V_{cu}	$5.2\,\mathrm{cm}^3$
Number of turns	N	120
Phase current	I_{RMS}	$0.69\,\mathrm{A}$
Average coil flux	Φ_{RMS}	$90\,\mu\mathrm{Wb}$
Iron losses	P_{Fe}	$0.2\,\mathrm{W}$
Copper losses	P_{Cu}	$0.7\,\mathrm{W}$
Efficiency	η	$90.5\,\%$

VI. Conclusion

This paper describes a method for shaping the cogging torque of a PM outrunner generator towards a desired sinusoidal torque pattern. The underlying goal of this approach is to compensate the cogging torque of a kinetic energy harvester (KEH, [18]) with the optimized counter cogging torque of the generator mechanically connected to the same shaft. Therefore, the total cogging torque can be highly reduced and a self-starting electromechanical energy harvester, comprising the KEH and the outrunner generator can be formed.

The key degree of freedom for shaping the cogging torque is the sinusoidal modulation of the machine's air gap. An algorithm based on the multi-dimensional Secant Method, which is related to the multi-dimensional Newton-Raphson Method, first evaluates the cogging torque of the current generator geometry with two-dimensional Finite Element Method (2-D FEM) simulations and then iterates the geometry of the outrunner machine until the cogging torque target is achieved. The air gap coefficients a_i and b_i describe the angular modulation of air gap with a sinusoidal basis, similar to a Fourier decomposition. Moreover, stator tooth width α_{FE} and angular distance between the rotor PMs α_{PMgap} are considered as geometry design parameters for the optimization.

The optimization results in a generator design with the desired sinusoidal cogging torque pattern and/or allows to achieve a total cogging torque reduction of the electromechanical energy harvester of 90%. Moreover, a brief electrical performance calculation reveals that the cogging torque shaping as proposed in this paper does not significantly degrade the machine's efficiency, which is calculated as $\eta = 90.5\,\%$ for the nominal operating point.

The presented cogging torque optimization is applied for an outrunner generator, providing self-starting capability of an electromechanical energy harvester, however, it can be a helpful tool for emerging applications in areas not directly linked to energy harvesting. A general, undesired repetitive torque ripple, induced by e.g. a mechanical power source, a mechanical load system or by the machine drive system can be eliminated by the counter cogging torque of an accordingly optimized PM machine.

VII. Acknowledgment

The authors would like to express their sincere appreciation to Nabtesco Corp., Japan, for the financial and technical support of research on energy harvesting technologies at the Power Electronic Systems Laboratory, ETH Zurich, which provided the basis for achieving the results presented in this paper. In particular, inspiring technical discussions with K. Nakamura and Y. Tsukada should be acknowledged.

References

[1] R. Krishnan, *Permanent magnet synchronous and brushless DC motor drives*. Taylor and Francis Group, 2010.

[2] W. Wu, "Disturbance Compensation for DC Motor Mechanism Low Speed Regulation: A Feedforward and Feedback Implementation," *Proceedings of the IEEE Conference on Decision and Control and European Control Conference (CDC)*, pp. 1614–1619, December 2011.

[3] D. G. Dorrell, M. F. Hsieh, M. Popescu, L. Evans, D. A. Staton, and V. Grout, "A Review of the Design Issues and Techniques for Radial-Flux Brushless Surface and Internal Rare-Earth Permanent-Magnet Motors," *IEEE Transactions on Industrial Electronics*, vol. 58, no. 9, pp. 3741–3757, September 2011.

[4] D. Wang, X. Wang, and S. Y. Jung, "Cogging Torque Minimization and Torque Ripple Suppression in Surface-Mounted Permanent Magnet Synchronous Machines using Different Magnet Widths," *IEEE Transactions on Magnetics*, vol. 49, no. 5, pp. 2295–2298, May 2013.

[5] N. Chen, S. L. Ho, and W. N. Fu, "Optimization of Permanent Magnet Surface Shapes of Electric Motors for Minimization of Cogging Torque using FEM," *IEEE Transactions on Magnetics*, vol. 46, no. 6, pp. 2478–2481, June 2010.

[6] I. Petrov, P. Ponomarev, Y. Alexandrova, and J. Pyrhönen, "Unequal Teeth Widths for Torque Ripple Reduction in Permanent Magnet Synchronous Machines with Fractional-Slot Non-Overlapping Windings," *IEEE Transactions on Magnetics*, vol. 51, no. 2, pp. 1–9, February 2015.

[7] S. H. Lee, Y. J. Kim, K. S. Lee, and S. J. Kim, "Multiobjective Optimization Design of Small-Scale Wind Power Generator with Outer Rotor Based on Box-Behnken Design," *IEEE Transactions on Applied Superconductivity*, vol. 26, no. 4, pp. 1–5, June 2016.

[8] W. Zhao, T. A. Lipo, and B. I. Kwon, "Torque Pulsation Minimization in Spoke-type Interior Permanent Magnet Motors with Skewing and Sinusoidal Permanent Magnet Configurations," *IEEE Transactions on Magnetics*, vol. 51, no. 11, pp. 1–4, November 2015.

[9] C. Studer, A. Keyhani, T. Sebastian, and S. K. Murthy, "Study of Cogging Torque in Permanent Magnet Machines," *Conference Record of the IEEE Industry Applications Conference*, vol. 1, pp. 42–49 vol.1, October 1997.

[10] Z. Q. Zhu and D. Howe, "Influence of Design Parameters on Cogging Torque in Permanent Magnet Machines," *IEEE Transactions on Energy Conversion*, vol. 15, no. 4, pp. 407–412, December 2000.

[11] S. Jurkovic, K. Rahman, B. Bae, N. Patel, and P. Savagian, "Next Generation Chevy Volt Electric Machines; Design, Optimization and Control for Performance and Rare-Earth Mitigation," *Proceedings of the IEEE Energy Conversion Congress and Exposition (ECCE)*, pp. 5219–5226, September 2015.

[12] M. S. Islam, S. Mir, and T. Sebastian, "Issues in Reducing the Cogging Torque of Mass-Produced Permanent-Magnet Brushless DC Motor," *IEEE Transactions on Industry Applications*, vol. 40, no. 3, pp. 813–820, May 2004.

[13] A. N. Patel, "Cogging Torque Minimization by Magnet Edge Inset Variation Technique in Radial Flux Surface Mounted Permanent Magnet Brushless DC (PMBLDC) Motor," *Proceedings of the Nirma University International Conference on Engineering (NUiCONE)*, November 2015.

[14] M. Lukaniszyn, M. JagieLa, and R. Wrobel, "Optimization of permanent magnet shape for minimum cogging torque using a genetic algorithm," *IEEE Transactions on Magnetics*, vol. 40, no. 2, pp. 1228–1231, March 2004.

[15] J. F. Gieras, *Permanent magnet motor technology*. CRC Press, 2009.

[16] W. Tong, *Mechanical design of electric motors*. Taylor and Francis Group, 2014.

[17] J. Bacher and G. Maier, "Actions to Increase the Cogging Torque and Effects of the Increased Cogging Torque to Permanent Magnet DC Motors," *Proceedings of the European Conference on Power Electronics and Applications (EPE)*, September 2005.

[18] M. Flankl, A. Tüysüz, I. Subotic, and J. W. Kolar, "Novel Contactless Axial-Flux Permanent-Magnet Electromechanical Energy Harvester," *Proceedings of the IEEE Applied Power Electronics Conference and Exposition (APEC)*, March 2016.

[19] A. Tüysüz, A. Looser, J. W. Kolar, and C. Zwyssig, "Novel Miniature Motors with Lateral Stator for a Wide Torque and Speed Range," *Proceedings of the Annual Conference of IEEE Industrial Electronics Society (IECON)*, pp. 1741–1747, November 2010.

[20] A. Tüysüz, "Novel Miniature Motors for Wide Speed and Torque Ranges," Ph.D. dissertation, ETH Zurich, 2014.

[21] E. Favre, L. Cardoletti, and M. Jufer, "Permanent-Magnet Synchronous Motors: A Comprehensive Approach to Cogging Torque Suppression," *IEEE Transactions on Industry Applications*, vol. 29, no. 6, pp. 1141–1149, November 1993.

[22] Y. Zhang and J. Zhu, "A Novel Duty Cycle Control Strategy to Reduce Both Torque and Flux Ripples for DTC of Permanent Magnet Synchronous Motor Drives with Switching Frequency Reduction," *IEEE Transactions on Power Electronics*, vol. 26, no. 10, pp. 3055–3067, October 2011.

[23] M. Flankl, A. Tüysüz, and J. W. Kolar, "Analysis and Power Scaling of a Single-Sided Linear Induction Machine for Energy Harvesting," *Proceedings of the IEEE Industrial Electronics Society Conference (IECON)*, November 2015.

[24] V. S. Ryaben'kii and S. V. Tsynkov, *A theoretical introduction to numerical analysis*. CRC Press, 2007.

[25] M. Hanke-Bourgeois, *Grundlagen der Numerischen Mathematik und des Wissenschaftlichen Rechnens (in German)*. Vieweg+Teubner, 2009.